GEOCHEMISTRY

Dominance of benthic fluxes in the oceanic beryllium budget and implications for paleo-denudation records

Kai Deng[1]*, Jörg Rickli[1], Tim Jesper Suhrhoff[1], Jianghui Du[1], Florian Scholz[2], Silke Severmann[3], Shouye Yang[4], James McManus[5], Derek Vance[1]

The ratio of atmosphere-derived ^{10}Be to continent-derived ^{9}Be in marine sediments has been used to probe the long-term relationship between continental denudation and climate. However, its application is complicated by uncertainty in ^{9}Be transfer through the land-ocean interface. The riverine dissolved load alone is insufficient to close the marine ^{9}Be budget, largely due to substantial removal of riverine ^{9}Be to continental margin sediments. We focus on the ultimate fate of this latter Be. We present sediment pore-water Be profiles from diverse continental margin environments to quantify the diagenetic Be release to the ocean. Our results suggest that pore-water Be cycling is mainly controlled by particulate supply and Mn-Fe cycling, leading to higher benthic fluxes on shelves. Benthic fluxes may help close the ^{9}Be budget and are at least comparable to, or higher (~2-fold) than, the riverine dissolved input. These observations demand a revised model framework, which considers the potentially dominant benthic source, to robustly interpret marine Be isotopic records.

INTRODUCTION

Earth's environment gradually moved from greenhouse conditions to an icehouse state in the Cenozoic, concurrent with a decline in atmospheric CO_2 concentrations (*1*, *2*). A long-standing hypothesis to explain these observations invokes enhanced removal of CO_2 from the atmosphere via increased silicate weathering. It is further posited that this weathering is driven by mountain uplift and erosion as inferred from an increase in oceanic isotope ratios of elements such as strontium (^{87}Sr/^{86}Sr) and lithium (^{7}Li/^{6}Li) (*3*, *4*). However, it is also well-established that a small excess of CO_2 output by silicate weathering (C sink) relative to volcanic degassing (C source) could potentially remove all atmospheric CO_2 in a few million years (*5*). Recent studies have sought to resolve this controversy in two ways, by invoking either CO_2 release from a compensatory source (*6*) or an increase in the weathering feedback strength without requiring a higher weathering flux (*7*, *8*).

In recent years, marine sedimentary records of beryllium isotopes (^{10}Be/^{9}Be) have been used as a tracer for continental denudation, which is the sum of chemical weathering and physical erosion (*9*, *10*). Since estimates are available for the past atmospheric delivery of ^{10}Be to the oceans (*11*), the ratio can, in principle, quantify fluxes of ^{9}Be delivered by rivers in dissolved and particulate forms (*10*). Compared to other weathering tracers mentioned above (*3*, *4*), which may mostly be sensitive to weathering style and/or the isotope composition of the source rather than weathering flux, the major potential advantage of ^{10}Be/^{9}Be lies in its direct link with the continental input flux of ^{9}Be (*8*, *12*). The discrepancy between proxy behaviors might help explain the inconsistency between the marked change in Sr-Li isotopes and relatively stable ^{10}Be/^{9}Be ratios. The latter proxy suggests a small variability in fluxes of chemical weathering and/or denudation in the late Cenozoic (*8*, *9*).

The promising applications of ^{10}Be/^{9}Be ratios are currently hampered by an incomplete understanding of the Be budget of the oceans, particularly the efficiency of ^{9}Be transmission through the continent-ocean interface (*13*, *14*). Recent modeling efforts have brought this uncertainty into the spotlight, emphasizing that different parametrizations of estuarine removal of dissolved ^{9}Be lead to contrasting expectations for the response of oceanic ^{10}Be/^{9}Be ratios to continental denudation (*15*, *16*). However, riverine dissolved ^{9}Be alone is insufficient to close the oceanic ^{9}Be budget (*14*, *16*). One potential missing source could be the early diagenetic release of particulate-bound reactive ^{9}Be deposited on continental margins (*10*, *14*). This benthic flux generated at the sediment-water interface is substantial for the marine budget of a number of other particle-reactive metals, such as iron (*17*) and rare earth elements (REE) (*18*).

A quantification of such benthic sedimentary fluxes is key to understanding the sensitivity of oceanic ^{10}Be/^{9}Be to changing continental denudation and/or weathering and the time scales on which the ocean responds to changes in continental inputs. However, direct constraints on benthic Be fluxes from marine pore-water data are extremely scarce (*19*) and still absent for continental shelves where most terrigenous sediment is deposited. Here, we present depth profiles of pore-water Be from different continental margins across variable water depth and redox conditions, which allow the derivation of a comprehensive quantitative constraint on this source. We seek to reveal the controls on pore-water Be concentrations and to quantify the benthic Be flux. We show that the benthic flux could be the major pathway by which ^{9}Be enters the dissolved pool of the oceans and provide an alternative interpretative framework for the small variability in Cenozoic Be isotopic records.

Sedimentary environment background

We studied stations in the East China Sea (depth: 6 to 46 m), the Baltic Sea (depth: 23 to 24 m), the Mexico margin (site: Soledad; depth: 542 m), and the California margin (sites: Catalina, San

[1]Institute of Geochemistry and Petrology, Department of Earth Sciences, ETH Zürich, Clausiusstrasse 25, 8092 Zürich, Switzerland. [2]GEOMAR Helmholtz Centre for Ocean Research Kiel, Wischhofstraße 1-3, 24148 Kiel, Germany. [3]Department of Marine and Coastal Sciences, Rutgers, The State University of New Jersey, New Brunswick, NJ 08901-8521, USA. [4]State Key Laboratory of Marine Geology, Tongji University, 200092 Shanghai, China. [5]Bigelow Laboratory for Ocean Sciences, 60 Bigelow Drive, East Boothbay, ME 04544, USA.
*Corresponding author. Email: kai.deng@erdw.ethz.ch

Clemente, and Patton Escarpment; depth: 1300 to 3707 m), covering a wide range of water depths from the continental shelf to the deep sea. These sites (Fig. 1 and table S1) are characterized by variable sedimentation rates (<0.1 to >10 mm/year) and redox conditions (oxic to anoxic), implying distinct diagenetic regimes.

The East China Sea shelf is one of the widest shelves worldwide, with a maximum width of >500 km and an area of ~5×10^5 km^2. It receives large amounts of terrestrial sediment, with sedimentation rates ranging from ~0.1 to >3 cm/year (*20*). The water column is dominantly oxic, with occasional occurrence of seasonal hypoxia (*21*). The Baltic Sea is one of the largest brackish water basins globally, and the studied Kiel Bight is a semi-enclosed basin in its southwest. It is at the other end of the redox scale, with anoxic and potentially sulfidic conditions commonly established at the sediment-water interface in summer through fall, that terminated in late fall by lateral advection of well-oxygenated water (*22*). Manganese and Fe shuttling takes place throughout the anoxic season. During the well-oxygenated season, terrigenous Mn and Fe oxides are also likely to be an important carrier phase for trace metals to the sediments (*23*). The major sediment source in the Kiel Bight is erosion of proximal coastal cliffs (*24*), resulting in a sedimentation rate of 0.2 to 0.9 cm/year (*25*). The Californian and Mexican margin sites encompass a range of redox situations broadly intermediate between the above two sites as well as a broad spectrum of particulate input. Soledad on the slope of the Mexico margin is characterized by anoxic conditions in bottom water and reduced particulate Mn supply to the sediments (*26*, *27*). The southern California margin sites (slope to deep sea) see bottom water conditions ranging from hypoxia to well oxygenated (bottom water O_2: 19 to 132 μmol/liter) and sediment accumulation rates ranging from 3 to 15 mg cm^{-2} $year^{-1}$ (*28*).

RESULTS

Pore-water Be and its controls

At each sampling station, pore-water samples were separated from core sediments at ~cm resolution for the preconcentration and determination of Be concentrations. A detailed description of the sampling and analysis is provided in Materials and Methods. Pore-water and bottom water Be concentrations, together with Mn and Fe concentrations, are presented in Fig. 2 and table S2. Pore-water Be concentrations ($[Be]_{diss}$) range from seawater-like values of ~20 pM to a maximum of ~1000 pM. At shallow depths (e.g., <5 cm), $[Be]_{diss}$ is commonly elevated compared to bottom water or near-interface pore-water (Fig. 2). This observation suggests that pore-water Be is released from sediments into overlying seawater. In general, pore-water $[Be]_{diss}$ reaches the highest values in the Baltic Sea (685 pM on average), intermediate values in the East China Sea (239 pM), and lowest values in the California (60 pM) and Mexico (46 pM) margins. At most stations, $[Be]_{diss}$ shows little variability at depth in contrast to its rapid rise just beneath the sediment-water interface.

Labile Be is mainly bound with reactive Mn-Fe oxyhydroxides in riverine and marine sediments (*29*, *30*). On the East China Sea shelf, the pore-water peak in $[Fe]_{diss}$ or $[Mn]_{diss}$ generally shallows with increasing water depth, together with a decrease in maximum concentration (Fig. 2). These features are also observed for $[Be]_{diss}$, suggesting a Be source linked to Mn-Fe mobilization through reduction. Likewise, $[Be]_{diss}$ and $[Mn]_{diss}$ show similar increases at shallow core depth (≤6 cm) in the Baltic Sea. However, the slight decrease in $[Mn]_{diss}$ at depth and overall low $[Fe]_{diss}$ point to sinks for both elements, such as Mn carbonate and Fe sulfide (*23*). These sinks do not appear to affect $[Be]_{diss}$.

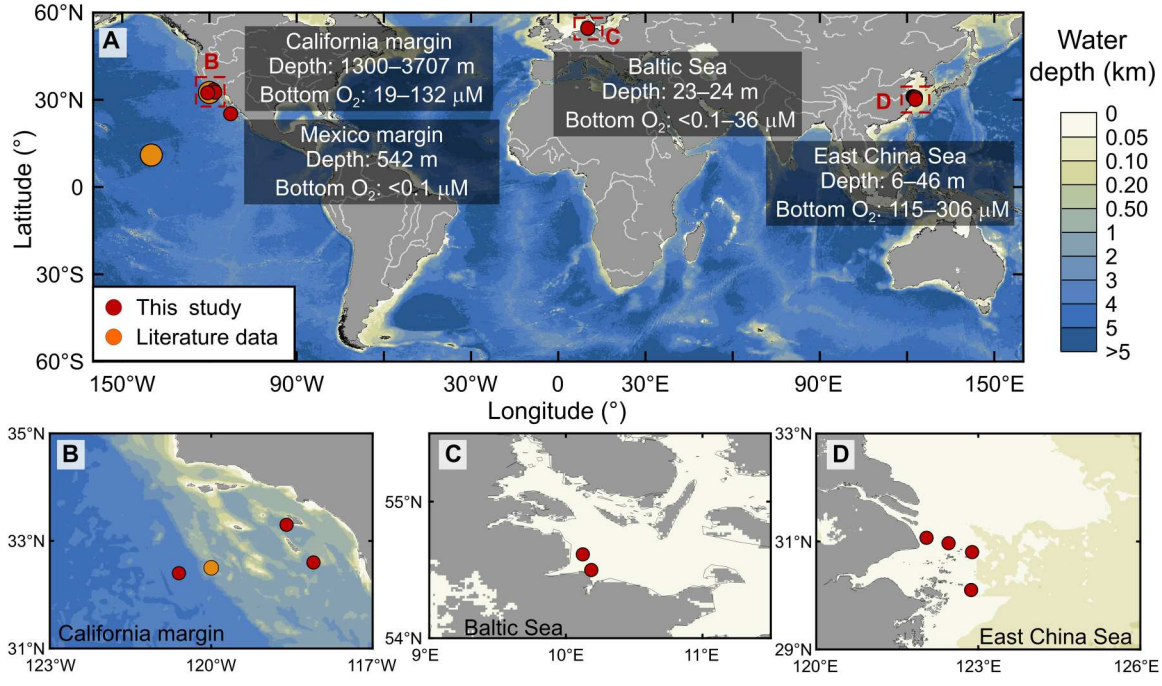

Fig. 1. Pore-water sampling stations. (**A**) An overview of all the stations with pore-water Be data. Basic information on each station is provided in table S1. Locations with literature pore-water Be data are also shown (*19*). Study regions with more than one sampling station are enlarged, including (**B**) the California margin, (**C**) the Baltic Sea, and (**D**) the East China Sea.

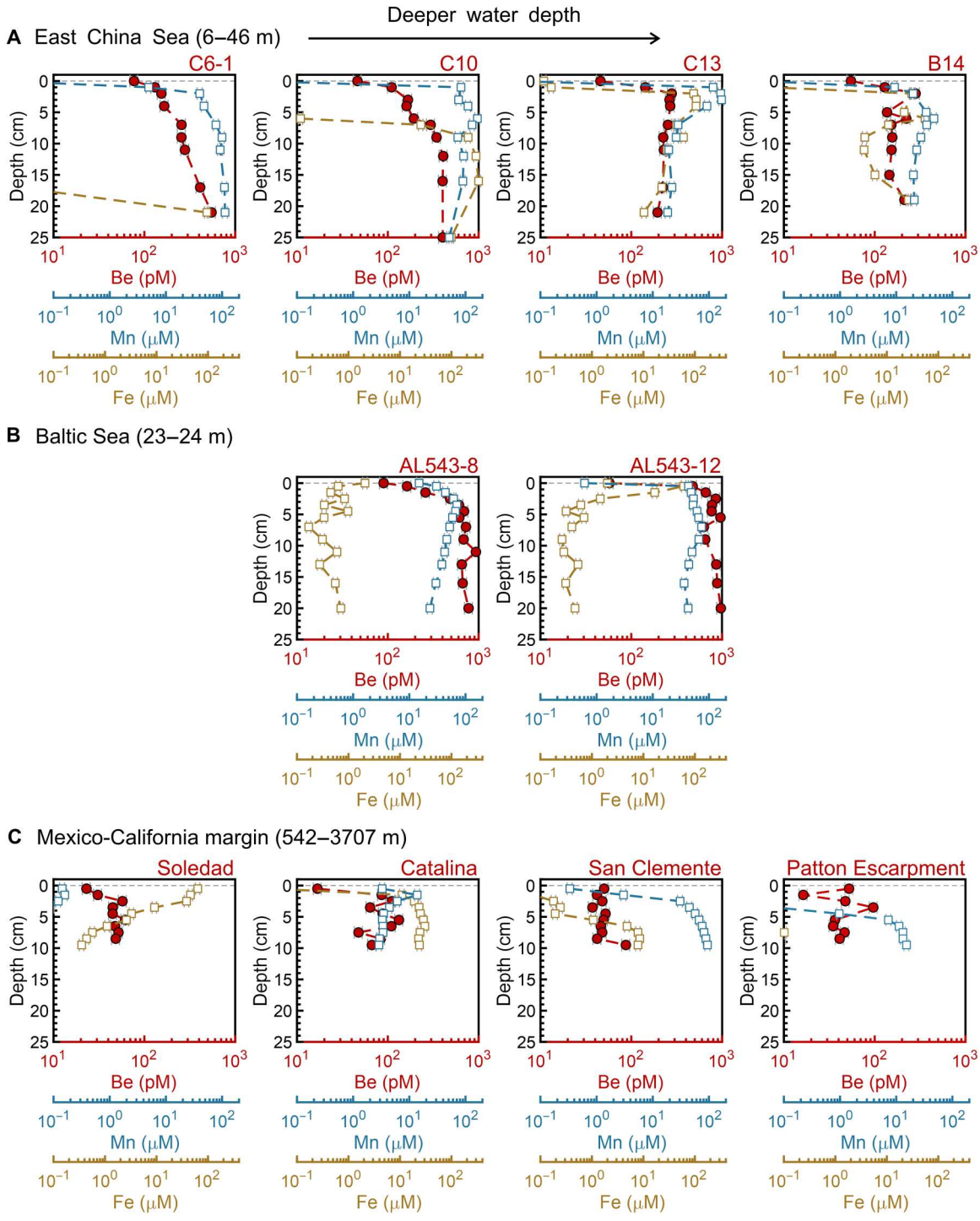

Fig. 2. Pore-water and bottom seawater Be, Mn, and Fe concentrations. Dissolved metal concentrations are shown for stations in (**A**) the East China Sea, (**B**) the Baltic Sea, and (**C**) the Mexico-California margin. Bottom water samples are plotted at a depth of 0 cm (gray dashed line). Note that the *x* axis is on a log scale.

For the Mexico-California margin sites, the depth profiles of $[Be]_{diss}$ do not correlate as closely with those of $[Mn]_{diss}$ or $[Fe]_{diss}$, perhaps because of contrasting cycling processes for Fe and Mn at these sites. For example, negligible $[Mn]_{diss}$ in Soledad is due to limited Mn oxide supply from the water column (*26*), while negligible $[Fe]_{diss}$ in Patton Escarpment is explained by a deep O_2 penetration depth and low organic carbon remineralization rate (*28*). Hence, changes in individual sources and sinks of each element may obscure the link between Be and Mn or Fe. Nevertheless, Fig. 3 illustrates a systematic relationship between pore-water Be and Mn during early diagenesis: $[Be]_{diss}$ remains at relatively low levels under low $[Mn]_{diss}$, while it strongly increases when reduction

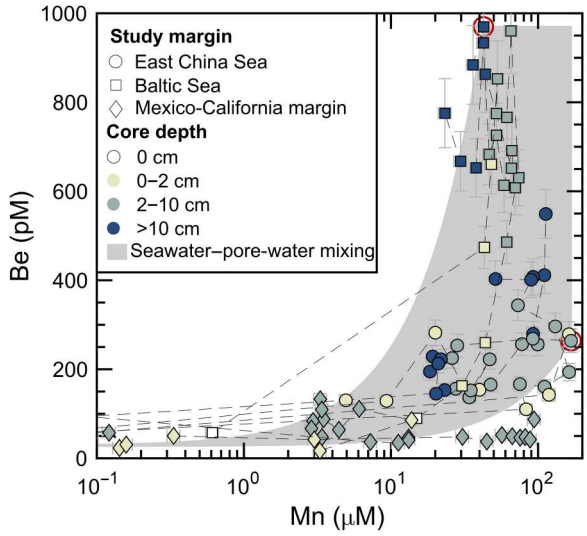

Fig. 3. Pore-water concentrations of Be versus Mn. Note that the *x* axis is on a log scale. The envelope of seawater–pore-water mixing is modeled using a seawater end-member, i.e., Pacific deep water (*55*, *56*), and two high $[Be]_{diss}$-$[Mn]_{diss}$ pore-water end-members that are potentially dominated by Mn reduction. Sources and sinks of Mn and Be do not entirely overlap. For example, formation of Mn carbonate could cause decrease in $[Mn]_{diss}$ (*23*) at high $[Be]_{diss}$. Hence, we include two scenarios using a pore-water sample with the highest $[Mn]_{diss}$ and another with the highest $[Be]_{diss}$ (red circles), leading to the lower and upper limits of the envelop, respectively.

of Mn oxides is prominent. Most samples fall within an envelope explained by mixing between a seawater end-member and two pore-water end-members whose sources are potentially located at the depth of Mn reduction.

Overall, $[Be]_{diss}$ is much lower on the continental slope and in the deep sea than on the shelf (Fig. 2). We suggest that abundant particle supply (*20*), in particular, Mn-Fe oxides (*23*), coupled to strong redox cycling in pore-water, could play a major role in the strong diagenetic Be release on the continental shelf.

Benthic Be fluxes in the oceans

We calculate the diffusive flux of Be across the sediment-water interface at each station (Fig. 4A), using Fick's first law and the pore-water $[Be]_{diss}$ gradient (details in Materials and Methods). Literature data from two deep-sea stations are included (*19*). The diffusive Be flux varies over two orders of magnitude, ranging from 0.8 pmol cm^{-2} $year^{-1}$ at the Mexico margin to 85.5 pmol cm^{-2} $year^{-1}$ in the Baltic Sea (AL543-12). If diffusive Be fluxes were strictly controlled of the oxidation-reduction potential of the sediment package, then they would be negatively correlated with bottom water O_2, but such correlation is insignificant in our dataset ($P > 0.1$; Fig. 4A). For example, in the Baltic Sea, the suboxic site shows a higher flux than the anoxic site, potentially because it is located within a submarine channel and may receive more terrestrial sediment (*31*). At the Mexico-California margins, the lower Be flux in anoxic Soledad is likely caused by limited Mn and Be supply from the water column (*26*). Nevertheless, any potential relationship between sediment supply and diffusive Be flux cannot easily be inferred from our dataset. For example, the diffusive Be fluxes show a small range (2.7 to 3.2 pmol cm^{-2} $year^{-1}$) at the three Californian margin sites despite a fivefold variability in sedimentation rates (*28*).

In brief, benthic Be fluxes on shelves are much higher than those on the slope and in the deep sea (Fig. 4A), consistent with the general spatial pattern of, e.g., benthic Mn fluxes (*32*). Furthermore, advection caused by bioirrigation and dynamic hydrological conditions, rather than diffusion, may dominate benthic fluxes of trace metals on shelves (*33*), suggesting that the actual fluxes could be even higher than diffusion-based estimates. Hence, our observations argue for an important role of continental shelves in the benthic Be source.

DISCUSSION

Updated framework of oceanic Be cycling

On the basis of pore-water data from this study and from the literature (*19*), a first-order estimate of the global benthic Be flux can be provided. We use benthic Be fluxes at a range of stations (table S3) for areal extrapolation at different water depth intervals. For global continental shelves (0 to 200 m), the studied East China Sea shelf, as one of the widest shelves worldwide (~2% of global shelf area), is adopted as the representative setting. When calculating the benthic Be flux on shelves, advection processes including bioirrigation and kinetic energy dissipation from, e.g., shear flow (*33*) need to be taken into account. Here, this is done by multiplying the change in $[Be]_{diss}$ across the sediment-water interface by the advective water exchange rate (v) determined around our study region using $^{224}Ra/^{228}Th$ disequilibria (Eqs. 3 and 4 and Materials and Methods) (*33*). The suggested shelf benthic Be flux for areal extrapolation is 140 ± 107 pmol cm^{-2} $year^{-1}$, much higher than the diffusion-based estimates at the same stations of the East China Sea shelf as expected (13.9 ± 4.2 pmol cm^{-2} $year^{-1}$; table S3). We consider this advection-based estimate to be reasonable, because the range of v on shelves used here (18 ± 13 m/year) agrees well with the range of the apparent pore-water exchange velocity across the sediment-water interface (2 to 34 m/year) calculated from several shelf settings in North America (*34*–*36*).

At deeper water depth, the global benthic flux on the slope and in the deep sea (water depth: 0.2 to 4 km) is calculated as the average diffusive flux at three nonanoxic stations (1300 to 3707 m) on the California margin (2.9 ± 0.3 pmol cm^{-2} $year^{-1}$; Fig. 4A). In addition, the global benthic flux in the abyssal basins (>4 km) is derived from the diffusive flux in the deep Pacific at 4910 m (1.4 ± 0.2 pmol cm^{-2} $year^{-1}$) (*19*). In general, the sedimentary (sedimentation rate) and diagenetic (related to organic carbon delivery/oxidation) environments at the selected stations are close to globally representative conditions at the corresponding depth intervals or fall within the representative parameter range (table S4). The calculation of a global-scale flux estimate based on areal extrapolation (*37*) is given in table S5. When only considering diffusion processes over the global scale as a conservative estimate, the total benthic Be input is calculated as $1.1 \pm 0.1 \times 10^7$ mol/year. In comparison, after accounting for advection processes on shelves, the global integrated benthic Be input reaches $4.5 \pm 2.9 \times 10^7$ mol/year. In particular, continental shelves with abundant terrestrial particle supply account for 84% of the total benthic source.

We revisit the oceanic Be budget based on these updated constraints on the benthic source (Fig. 4B; calculation details in table S5). The oceanic Be sources include riverine dissolved loads,

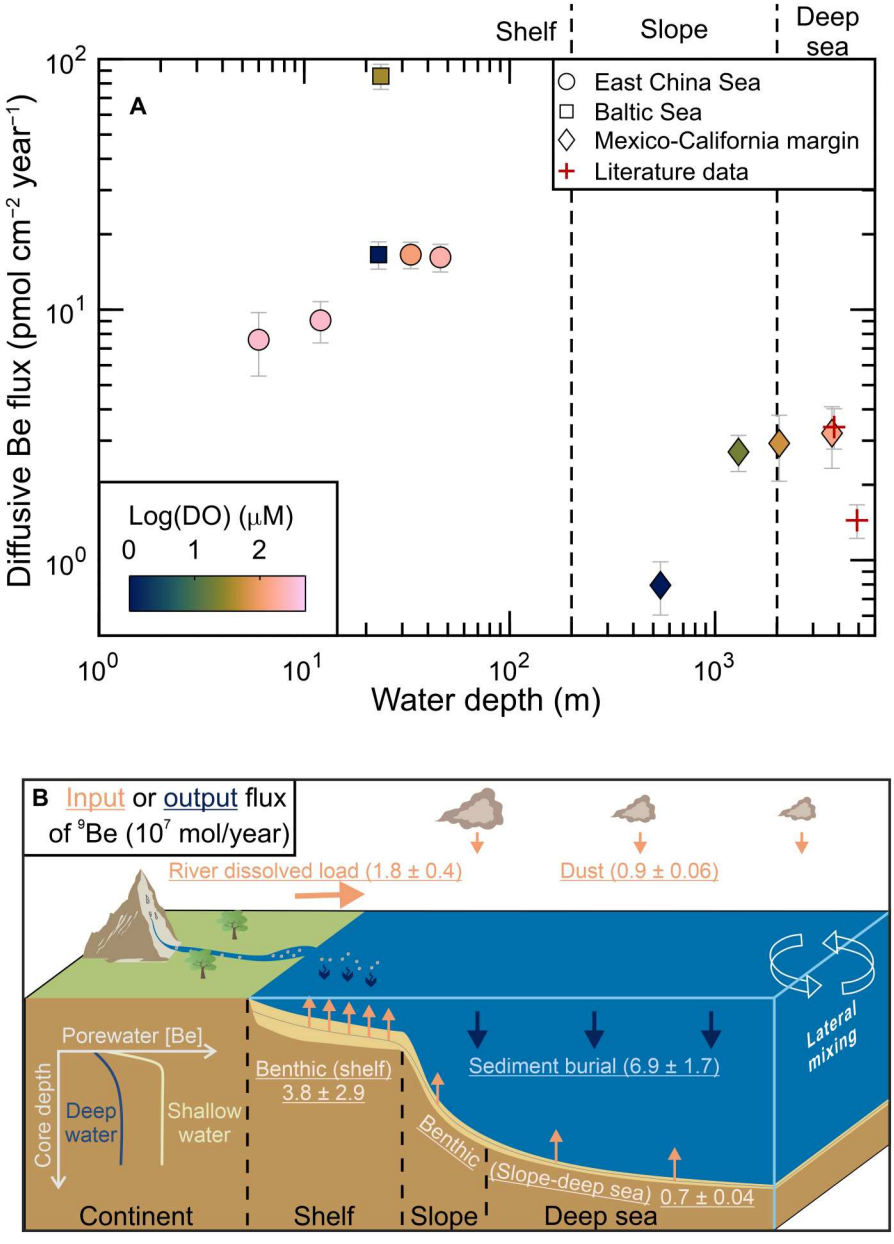

Fig. 4. Updated framework of oceanic Be cycling. (**A**) Diffusive sedimentary Be flux variation with water depth. The symbols are colored by bottom water O_2 (DO). Axes and color bars are on a log scale. Literature data (red crosses) are from (*19*). Details on flux calculations are provided in table S3. (**B**) First-order estimate of oceanic Be budget. The major sources are river dissolved load, eolian dust, and benthic flux, while the major sink is sediment burial. Inputs (7.2 ± 2.9 × 10^{7} mol/year) and outputs (6.9 ± 1.7 × 10^{7} mol/year) match within uncertainty. Calculation details and references are provided in table S5.

eolian dust, and benthic fluxes, while the major sink is scavenging onto marine particulates. The effective riverine input to the oceans (1.8 ± 0.4 × 10^{7} mol/year) is calculated using compiled riverine dissolved Be flux data (table S6) and the average estuarine removal (56%) (*14*). The dust input (0.9 ± 0.06 × 10^{7} mol/year) is estimated using the global dust flux (*38*), the Be concentration in dust same as that of the upper continent crust (*39*), and the soluble fraction (~9%) of dust Be (*13*). The diffusion-based benthic Be fluxes are of the same magnitude as the riverine input and would account for 28% of the total oceanic Be input. If advective fluxes on shelves are included as estimated above, then the benthic input becomes the largest source to the oceans (62% of the total input on average) and ~2-fold higher than the effective riverine dissolved input.

The sediment burial output of ^{9}Be (6.9 ± 1.7 × 10^{7} mol/year) can be calculated (*40*) on the basis of global atmospheric ^{10}Be input (assuming a negligible continental ^{10}Be input; see the sensitivity test in the Supplementary Materials), the assumption of input-output balance for oceanic ^{10}Be, and the global average deep-sea ^{10}Be/^{9}Be (*10*, *41*). This estimate of oceanic ^{9}Be output, if valid, would result in an oceanic ^{9}Be residence time of 485 ± 120 year, which falls within the range for the ocean-wide scavenging residence time of Be (480

to 1250 years) estimated by other methods (*42*, *43*). Because the ^{9}Be sources ($7.2 \pm 2.9 \times 10^{7}$ mol/year in total) and the ^{9}Be sink are constrained by independent approaches, it is encouraging that they agree within uncertainty (<10% mismatch; Fig. 4B).

Given different scenarios for the benthic flux calculation and the uncertainty therein, we perform a sensitivity analysis on their effect on the resulting benthic ^{9}Be input and the ratio of benthic to riverine ^{9}Be input (fig. S2). The calculated benthic ^{9}Be flux through diffusion processes only (1.1×10^{7} mol/year) is equivalent to ~60% of the riverine dissolved input. This flux estimate is in itself substantial but not enough to close the oceanic ^{9}Be budget, which requires an input flux of $4.2 \pm 1.7 \times 10^{7}$ mol/year from sources other than rivers and dust according to the ^{9}Be burial output (table S5). In comparison, the benthic flux that takes advection on shelves into account ($4.5 \pm 2.9 \times 10^{7}$ mol/year) would meet the required missing source. Even when considering the large uncertainty propagated from estimates on water advection, the benthic flux is close to, or higher than, the riverine dissolved load (minimum ratio: 0.8; average ratio: 2.4) and accounts for 62 ± 16% of the total ^{9}Be input. In addition, a fraction of pore-water trace metals released via water advection might immediately be rescavenged near the sediment-water interface (*44*). It is difficult to quantify the effect of this process without in situ observations. However, on the basis of our constraints on ^{9}Be mass balance, a minimum benthic flux that could be affected by rescavenging and still meet the total ^{9}Be output within uncertainty (lower bound: 5.2×10^{7} mol/year; table S5) is 2.4×10^{7} mol/year. Even in this case, the benthic flux that ultimately enters the ocean is 130% of the riverine dissolved load and 47% of the total input (fig. S2), emphasizing its potential control on oceanic Be cycling.

Implications for the Cenozoic oceanic Be isotopic records

The updated framework for the oceanic Be budget (Fig. 4B) is valuable for the interpretation of marine isotope records. Recent debate has centered on the uncertainties in the riverine dissolved input and its estuarine removal (*15*, *16*). However, in the budget presented above, this riverine dissolved source is not the most important and may not control variability in paleo-records. Secular records are here predicted to respond more to the benthic source, either in a diffusion-only scenario or more plausibly in a scenario including advection processes on shelves. In addition, because pore-water Be only reflects a minor fraction (<0.1%) of the sediment reactive pool (e.g., ~20% of bulk sediment Be) (*10*), the benthic source has the potential to change with time in response to sedimentary processes. Key factors might include (i) changing pore-water Mn-Fe redox cycling, potentially controlled by organic carbon delivery (*32*), and perhaps (ii) changing sediment delivery (*10*). Both processes are likely dynamic on continental shelves and would respond to environmental changes (e.g., sea-level fluctuation), although the relative importance of each process is still to be established.

Late Cenozoic ^{10}Be/^{9}Be records show minor temporal variability (relative SD of ocean ^{9}Be input: 20 to 30%) and have been interpreted in terms of a relatively stable rate of continental denudation and/or weathering (*8*–*10*). However, because the riverine dissolved input is unlikely to be a major ^{9}Be source, we suggest that there are alternative views of the paleo-isotope records. For example, if the benthic source is kept constant at 4.5×10^{7} mol/year, then a ~2-fold increase in denudation rate in the late Cenozoic [inferred from, e.g., globally compiled thermochronometric age data (*45*) and modeling results (*8*) based on C-Li-Be-S-O data], together with the assumption of a linear relationship between effective riverine dissolved input and denudation rate (*10*), would lead to an increase of less than 20% in the total ^{9}Be input, consistent with the minor paleo-record variability. Moreover, a potential decrease in the benthic source resulting from the sea-level fall and smaller shelf area in the late Cenozoic (*46*) could counterbalance an increase in riverine dissolved input. Overall, the realization of a substantial benthic flux of Be implies a more indirect and complex response of oceanic ^{9}Be to continental denudation fluxes than previously assumed (*15*, *16*). The paleo-records of oceanic ^{10}Be/^{9}Be may not mimic the evolution of one single source. Instead, individual sources—benthic processes, rivers, and dust—could show different responses to climatic-tectonic factors, with their integrated effect potentially resulting in the observed small oceanic ^{10}Be/^{9}Be variability back through time (*9*).

Overall, our marine pore-water Be results provide direct evidence for a benthic Be flux to overlying seawater over the full depth range of the ocean basins (shelf-slope-deep sea). This benthic source provides a resolution to the oceanic Be imbalance, and it may dominate the present-day oceanic input. More marine pore-water Be data, especially on advection-dominated continental shelves, will still be required to refine our proposed Be budget and reduce the flux uncertainty. On the basis of this updated framework for the oceanic Be budget, we propose that oceanic Be cycling may be governed "bottom-up" (benthic process) rather than "top-down" (river or dust) (*47*). Hence, the hypothesis of a dominant riverine dissolved Be input to the oceans needs to be revisited (*15*). Given the strong cycling of pore-water Be on shelves and distinct Be isotope ratios of marine and continental sources, Be isotopes may have the potential to distinguish between the two types of reactive pools in marine sediments, allowing the investigation of boundary exchange processes in the modern ocean (*48*, *49*). For a robust interpretation of open-ocean paleo-isotopic records, a revised model framework considering the potentially dominant benthic source is, however, still required.

MATERIALS AND METHODS

Details on pore-water Be separation and determination

At each sampling station, sediment cores (10 to 25 cm) were retrieved using multi- or mini-corers. Overlying bottom water was first drained and filtered. Pore-water was separated using methods previously described in detail (*31*, *50*) at ~cm resolution, either by centrifuging sliced core sediment under anaerobic conditions followed by filtration (Baltic Sea samples: 0.2-μm filters and Mexico-California margin samples: 0.45-μm filters) or by in situ extraction via precleaned Rhizon samplers (East China Sea samples: 0.15-μm filters). Water samples were acidified for storage (pH ≤ 2).

Separation and determination of Be were performed at ETH Zürich. Beryllium measurement in pore-water samples is analytically challenging due to the low concentrations (picomol/liter level) and the small available sample volumes (e.g., several milliliters). We developed a procedure that can separate three components, which are, salt matrix, Be, and other trace metals such as REE on the same sample, optimizing the usage of precious pore-water samples. To do so, we coupled a well-established REE

preconcentration protocol (*50*, *51*) with an additional procedure for the preconcentration of Be from the remaining seawater matrix (*14*, *52*).

About 5 to 20 ml of filtered and acidified pore- or seawater was used to preconcentrate most trace metals (called TM fraction) using ethylenediaminetriacetic acid chelating resin, i.e., NOBIAS PA1 (*51*). Concentrated ammonium acetate buffer was added to each sample to reach an acetic acid concentration of 0.1 M, and the sample pH was adjusted to 5.5 to 6.0 using concentrated ammonia and HCl. Subsequently, samples were loaded onto pre-cleaned and preconditioned NOBIAS columns with a resin bed of ~100 μl, and the matrix cations were eluted from the column with 16 to 20 ml of 30 mM ammonium acetate buffer. The loaded sample and the matrix-eluting buffer solutions were collected as the B fraction. Beryllium is overwhelmingly in this fraction (> ~95%) (*51*), as it is commonly not retained by the resin at a pH of 5.5 to 6.0. Trace metals including REE (TM fraction) were lastly eluted from the resin in 4 ml of 1 M HCl.

We added $FeCl_3$ in concentrated HCl immediately to the B fractions to lower the pH to <2, and the samples were shaken for some time to reach equilibrium. Beryllium was then coprecipitated with Fe hydroxides at a pH of 7.5 to 8.2. After >12 hours with mild shaking, the precipitates were separated from the supernatants by centrifugation and rinsed twice with pH-adjusted Milli-Q water (pH = ~8). Beryllium was separated from Fe using anion resin (AG MP-1, 1-ml resin bed), and the dried B fraction was oxidized using 14.5 M HNO_3 and 30 volume % H_2O_2. An additional purification step using cation resin (AG 50W-X8, 0.8-ml resin bed) was applied (*53*) to further reduce remaining matrix cations such as Ca and Mg in the B fraction.

Beryllium concentrations of the B fractions were measured in 0.5 to 1 ml of 2% HNO_3 doped with 1 part per billion of indium (as an internal standard) on a Thermo Fisher Element XR [inductively coupled plasma mass spectrometry (ICP-MS)] in low-resolution mode. Given the low Be concentrations, the ICP-MS was coupled with a desolvating sample introduction system (Aridus 1) to boost instrument sensitivity and to increase the signal-to-noise ratio. The intensity data were corrected for machine blank and machine drift. Final Be concentrations were also corrected for procedural blanks of the corresponding batches, which reflect the Be accumulated during chemical processing and account for ~2% of the average [Be] of all samples (0.05 ± 0.05 parts per trillion, 1 SD; n = 16; the processed volume is the same as the sample volume of the given batch). Note that the TM fractions were also measured for Be concentrations using an ICP-MS setup as described in (*50*) to check whether a minor amount of Be was retained on the NOBIAS PA1 resin. When this fraction of Be was not negligible (accounting for ~6% of total [Be] on average), it was added to the Be measurement of the B fraction to derive a final Be concentration.

An in-house seawater standard Jstd-1 of known Be concentration (1 nM) (*14*) was processed in each sample batch to assess accuracy and precision. The total Be amount of each standard processed (from 5 to 10 ml of solution) is similar to that of the pore-water samples with high Be concentrations. The average Be yield of this standard was 95 ± 8% (n = 11, 1 SD). Hence, we propagated a relative uncertainty of 10% for all pore-water Be measurements.

In addition, an aliquot of each original pore-water sample was diluted ~40 times for the determination of Fe and Mn concentrations. Accuracy and precision were assessed using river standard SLRS-6 from the National Research Council Canada. Repeat measurements of SLRS-6 show an SD of <10% and also agree with certified values within ~10%. All element concentrations were measured using a Thermo Fisher Element XR at ETH Zürich, except Mn data in the Baltic Sea that were measured at GEOMAR (Germany) using ICP optical emission spectrometry (VARIAN 720-ES). Note that pore-water Fe and Mn data from the stations in the East China Sea were published before (*50*).

Calculation of benthic Be flux

Early diagenetic reactions can produce a $[Be]_{diss}$ gradient in sediment pore-waters, which is used for quantifying the diffusive Be flux ($J_{Be-diff}$) following Fick's first law of diffusion (*36*)

$$J_{Be-diff} = \varphi \times D_{Be}^{sed} \times \frac{\partial C_{Be}}{\partial z} \quad (1)$$

where $\frac{\partial C_{Be}}{\partial z}$ is the maximum concentration gradient in Be from shallow pore-water to bottom water (mol liter^{-1} cm^{-1}) in the pore-water profile, φ is the porosity (assuming as a constant of 0.9) (*19*, *54*), and D_{Be}^{sed} is the effective diffusion coefficient of Be in sediments (cm^2/s). D_{Be}^{sed} is calculated using the diffusion coefficient of Be in seawater (D_{Be}^{sw} in cm^2/s) and tortuosity (θ^2; estimated from porosity as given in the denominator of Eq. 2) (*36*)

$$D_{Be}^{sed} = \frac{D_{Be}^{sw}}{1 - \ln(\varphi^2)} \quad (2)$$

The empirical relationship between D_{Be}^{sw} and bottom water temperature (T in degrees Celsius) is provided by Boudreau (*36*), i.e., $D_{Be}^{sw} = (2.57 + 0.14\ T) \times 10^{-6}$ cm^2/s (R^2 = 0.99), and applied here, and site-specific D_{Be}^{sed} is provided in table S3. Diffusive Be fluxes from this study and the literature are provided in table S3.

In an advection-dominated setting, additional processes, e.g., bioirrigation and shear flow, can dominate solute exchange across the sediment-water interface. The advection-based Be flux (J_{Be-add}) is then calculated by the equation modified from (*33*)

$$J_{Be-add} = \nu \times \Delta[Be] \quad (3)$$

where Δ[Be] is the concentration difference between uppermost pore-water (1 cm) and bottom seawater, and ν is the interfacial water exchange rate (in m^3 m^{-2} d^{-1}). An exponential relationship between water depth (Z in meters) and ν determined from $^{224}Ra/^{228}Th$ disequilibria was proposed in China coastal seas (*33*). We here reprocessed the literature data (*33*) to generate a data fit and an estimate of its uncertainty (Eq. 4 and fig. S1).

$$\nu = 0.049 + 0.856e^{-0.134Z} \quad (4)$$

The coefficient of determination (R^2) of the fit is 0.97, and the root mean square error is 0.030. To estimate the advective Be flux on the shelf, we first calculated the mean gradient in $[Be]_{diss}$ at the sediment-water interface from the East China Sea stations at a water depth of ≥12 m, where pore-water depth patterns of Be (Fig. 2) and REE (*50*) are similar. We then multiplied this gradient with the advective water flux (0.049 ± 0.036 m^3 m^{-2} d^{-1}) derived from Eq. 4 for the global average shelf depth (65 m) (*37*), which is similar to the average depth of the East China Sea shelf (72 m). Overall, ν is relatively stable at ~0.05 m^3 m^{-2} d^{-1} when Z is >40 m.

Supplementary Materials

This PDF file includes:

Supplementary Text
Figs. S1 and S2
Tables S1 to S6
References

REFERENCES AND NOTES

1. J. W. B. Rae, Y. G. Zhang, X. Liu, G. L. Foster, H. M. Stoll, R. D. M. Whiteford, Atmospheric CO_2 over the past 66 million years from marine archives. *Annu. Rev. Earth Planet. Sci.* **49**, 609–641 (2021).
2. J. Zachos, M. Pagani, L. Sloan, E. Thomas, K. Billups, Trends, rhythms, and aberrations in global climate 65 Ma to present. *Science* **292**, 686–693 (2001).
3. M. E. Raymo, W. F. Ruddiman, Tectonic forcing of Late Cenozoic climate. *Nature* **359**, 117–122 (1992).
4. S. Misra, P. N. Froelich, Lithium isotope history of Cenozoic seawater: Changes in silicate weathering and reverse weathering. *Science* **335**, 818–823 (2012).
5. R. A. Berner, K. Caldeira, The need for mass balance and feedback in the geochemical carbon cycle. *Geology* **25**, 955–956 (1997).
6. M. A. Torres, A. J. West, G. Li, Sulphide oxidation and carbonate dissolution as a source of CO_2 over geological timescales. *Nature* **507**, 346–349 (2014).
7. J. K. Caves, A. B. Jost, K. V. Lau, K. Maher, Cenozoic carbon cycle imbalances and a variable weathering feedback. *Earth Planet. Sci. Lett.* **450**, 152–163 (2016).
8. J. K. Caves, D. E. Ibarra, F. von Blanckenburg, Neogene cooling driven by land surface reactivity rather than increased weathering fluxes. *Nature* **571**, 99–102 (2019).
9. J. K. Willenbring, F. von Blanckenburg, Long-term stability of global erosion rates and weathering during late-Cenozoic cooling. *Nature* **465**, 211–214 (2010).
10. F. von Blanckenburg, J. Bouchez, River fluxes to the sea from the ocean's $^{10}Be/^{9}Be$ ratio. *Earth Planet. Sci. Lett.* **387**, 34–43 (2014).
11. K. Deng, H. Wittmann, F. von Blanckenburg, The depositional flux of meteoric cosmogenic ^{10}Be from modeling and observation. *Earth Planet. Sci. Lett.* **550**, 116530 (2020).
12. F. von Blanckenburg, J. Bouchez, D. E. Ibarra, K. Maher, Stable runoff and weathering fluxes into the oceans over Quaternary climate cycles. *Nat. Geosci.* **8**, 538–542 (2015).
13. E. T. Brown, C. I. Measures, J. M. Edmond, D. L. Bourlès, G. M. Raisbeck, F. Yiou, Continental inputs of beryllium to the oceans. *Earth Planet. Sci. Lett.* **114**, 101–111 (1992).
14. T. J. Suhrhoff, J. Rickli, K. Crocket, E. Bura-Nakic, D. Vance, Behavior of beryllium in the weathering environment and its delivery to the ocean. *Geochim. Cosmochim. Acta* **265**, 48–68 (2019).
15. S. Li, S. L. Goldstein, M. E. Raymo, Neogene continental denudation and the beryllium conundrum. *Proc. Natl. Acad. Sci. U.S.A.* **118**, e2026456118 (2021).
16. F. von Blanckenburg, J. Bouchez, J. K. Willenbring, D. E. Ibarra, J. K. C. Rugenstein, There is no Neogene denudation conundrum. *Proc. Natl. Acad. Sci. U.S.A.* **119**, e2202387119 (2022).
17. V. A. Elrod, W. M. Berelson, K. H. Coale, K. S. Johnson, The flux of iron from continental shelf sediments: A missing source for global budgets. *Geophys. Res. Lett.* **31**, L12307 (2004).
18. A. N. Abbott, B. A. Haley, J. McManus, C. E. Reimers, The sedimentary flux of dissolved rare earth elements to the ocean. *Geochim. Cosmochim. Acta* **154**, 186–200 (2015).
19. D. L. Bourlès, G. Klinkhammer, A. C. Campbell, C. I. Measures, E. T. Brown, J. M. Edmond, Beryllium in marine pore waters: geochemical and geochronological implications. *Nature* **341**, 731–733 (1989).
20. J. P. Liu, A. C. Li, K. H. Xu, D. M. Velozzi, Z. S. Yang, J. D. Milliman, D. J. DeMaster, Sedimentary features of the Yangtze River-derived along-shelf clinoform deposit in the East China Sea. *Cont. Shelf Res.* **26**, 2141–2156 (2006).
21. J. Zhu, Z. Zhu, J. Lin, H. Wu, J. Zhang, Distribution of hypoxia and pycnocline off the Changjiang Estuary, China. *J. Mar. Sys.* **154**, 28–40 (2016).
22. S. T. Lennartz, A. Lehmann, J. Herrford, F. Malien, H. P. Hansen, H. Biester, H. W. Bange, Long-term trends at the Boknis Eck time series station (Baltic Sea), 1957–2013: Does climate change counteract the decline in eutrophication? *Biogeosciences* **11**, 6323–6339 (2014).
23. F. Scholz, J. McManus, S. Sommer, The manganese and iron shuttle in a modern euxinic basin and implications for molybdenum cycling at euxinic ocean margins. *Chem. Geol.* **355**, 56–68 (2013).
24. E. Seibold, N. Exon, M. Hartmann, F.-C. Kögler, H. Krumm, G. Lutze, R. Newton, F. Werner, Marine geology of Kiel bay, in *Sedimentology of Parts of Central Europe, Guidebook VIII International Sedimentology Congress* (Kramer, 1971).
25. C. A. Nittrouer, G. R. Lopez, L. Donelson Wright, S. J. Bentley, A. F. D'Andrea, C. T. Friedrichs, N. I. Craig, C. K. Sommerfield, Oceanographic processes and the preservation of sedimentary structure in Eckernförde Bay, Baltic Sea. *Cont. Shelf Res.* **18**, 1689–1714 (1998).
26. J. McManus, W. M. Berelson, S. Severmann, R. L. Poulson, D. E. Hammond, G. P. Klinkhammer, C. Holm, Molybdenum and uranium geochemistry in continental margin sediments: Paleoproxy potential. *Geochim. Cosmochim. Acta* **70**, 4643–4662 (2006).
27. S. Bruggmann, S. Severmann, J. McManus, Geochemical conditions regulating chromium preservation in marine sediments. *Geochim. Cosmochim. Acta* **348**, 239–257 (2023).
28. W. M. Berelson, J. McManus, K. H. Coale, K. S. Johnson, T. Kilgore, D. Burdige, C. Pilskaln, Biogenic matter diagenesis on the sea floor: A comparison between two continental margin transects. *J. Mar. Res.* **54**, 731–762 (1996).
29. D. Bourlès, G. M. Raisbeck, F. Yiou, ^{10}Be and ^{9}Be in marine sediments and their potential for dating. *Geochim. Cosmochim. Acta* **53**, 443–452 (1989).
30. H. Wittmann, F. von Blanckenburg, J. Bouchez, N. Dannhaus, R. Naumann, M. Christl, J. Gaillardet, The dependence of meteoric ^{10}Be concentrations on particle size in Amazon River bed sediment and the extraction of reactive $^{10}Be/^{9}Be$ ratios. *Chem. Geol.* **318–319**, 126–138 (2012).
31. F. Scholz, J. Cheng, Z. Zhang, P. Vosteen, C. Siebert, M. Frank, Benthic-pelagic coupling and isotopic fractionation of barium in Kiel Bight, SW Baltic Sea. *Front. Mar. Sci.* **10**, 1101095 (2023).
32. J. McManus, W. M. Berelson, S. Severmann, K. S. Johnson, D. E. Hammond, M. Roy, K. H. Coale, Benthic manganese fluxes along the Oregon-California continental shelf and slope. *Cont. Shelf Res.* **43**, 71–85 (2012).
33. X. Shi, L. Wei, Q. Hong, L. Liu, Y. Wang, X. Shi, Y. Ye, P. Cai, Large benthic fluxes of dissolved iron in China coastal seas revealed by $^{224}Ra/^{228}Th$ disequilibria. *Geochim. Cosmochim. Acta* **260**, 49–61 (2019).
34. D. E. Hammond, C. Fuller, in *The use of radon-222 to estimate benthic exchange and atmospheric exchange rates in San Francisco Bay* (American Association for the Advancement of Science-Pacific Division, 1979).
35. D. Archer, A. Devol, Benthic oxygen fluxes on the Washington shelf and slope: A comparison of in situ microelectrode and chamber flux measurements. *Limnol. Oceanogr.* **37**, 614–629 (1992).
36. B. P. Boudreau, in *Diagenetic Models and Their Implementation* (Springer, Berlin, 1997), vol. 410.
37. B. Eakins, G. Sharman, Hypsographic curve of Earth's surface from ETOPO1 (NOAA National Geophysical Data Center, Boulder, CO, 2012).
38. T. D. Jickells, Z. S. An, K. K. Andersen, A. R. Baker, G. Bergametti, N. Brooks, J. J. Cao, P. W. Boyd, R. A. Duce, K. A. Hunter, H. Kawahata, N. Kubilay, J. laRoche, P. S. Liss, N. Mahowald, J. M. Prospero, A. J. Ridgwell, I. Tegen, R. Torres, Global iron connections between desert dust, ocean biogeochemistry, and climate. *Science* **308**, 67–71 (2005).
39. R. L. Rudnick, S. Gao, 3.01 - Composition of the Continental Crust A2 - Holland, Heinrich D, in *Treatise on Geochemistry*, K. K. Turekian, Ed. (Pergamon, Oxford, 2003), pp. 1–64.
40. F. von Blanckenburg, R. K. O'Nions, N. S. Belshaw, A. Gibb, J. R. Hein, Global distribution of beryllium isotopes in deep ocean water as derived from Fe Mn crusts. *Earth Planet. Sci. Lett.* **141**, 213–226 (1996).
41. U. Heikkilä, F. von Blanckenburg, The global distribution of Holocene meteoric 10Be fluxes from atmospheric models. Distribution maps for terrestrial Earths surface applications (GFZ Data Services, GFZ Potsdam, Germany, 2015).
42. T. L. Ku, M. Kusakabe, C. I. Measures, J. R. Southon, G. Cusimano, J. S. Vogel, D. E. Nelson, S. Nakaya, Beryllium isotope distribution in the western North Atlantic: A comparison to the Pacific. *Deep Sea Res. Part A Oceanogr. Res. Papers* **37**, 795–808 (1990).
43. R. F. Anderson, Y. Lao, W. S. Broecker, S. E. Trumbore, H. J. Hofmann, W. Wolfli, Boundary scavenging in the Pacific Ocean: A comparison of ^{10}Be and ^{231}Pa. *Earth Planet. Sci. Lett.* **96**, 287–304 (1990).
44. G. M. Patton, R. Francois, D. Weis, E. Hathorne, M. Gutjahr, M. Frank, K. Gordon, An experimental investigation of the acquisition of Nd by authigenic phases of marine sediments. *Geochim. Cosmochim. Acta* **301**, 1–29 (2021).
45. F. Herman, D. Seward, P. G. Valla, A. Carter, B. Kohn, S. D. Willett, T. A. Ehlers, Worldwide acceleration of mountain erosion under a cooling climate. *Nature* **504**, 423–426 (2013).
46. K. G. Miller, M. A. Kominz, J. V. Browning, J. D. Wright, G. S. Mountain, M. E. Katz, P. J. Sugarman, B. S. Cramer, N. Christie-Blick, S. F. Pekar, The Phanerozoic record of global sea-level change. *Science* **310**, 1293–1298 (2005).
47. B. A. Haley, J. Du, A. N. Abbott, J. McManus, The impact of benthic processes on rare earth element and neodymium isotope distributions in the oceans. *Front. Mar. Sci.* **4**, 426 (2017).
48. A. Bernhardt, M. Oelze, J. Bouchez, F. von Blanckenburg, M. Mohtadi, M. Christl, H. Wittmann, $^{10}Be/^{9}Be$ ratios reveal marine authigenic clay formation. *Geophys. Res. Lett.* **47**, e2019GL086061 (2020).

49. H. Wittmann, F. von Blanckenburg, M. Mohtadi, M. Christl, A. Bernhardt, The competition between coastal trace metal fluxes and oceanic mixing from the $^{10}Be/^{9}Be$ ratio: Implications for sedimentary records. *Geophys. Res. Lett.* **44**, 8443–8452 (2017).
50. K. Deng, S. Yang, J. Du, E. Lian, D. Vance, Dominance of benthic flux of REEs on continental shelves: Implications for oceanic budgets. *Geochem. Perspect. Lett.* **22**, 26–30 (2022).
51. Y. Sohrin, S. Urushihara, S. Nakatsuka, T. Kono, E. Higo, T. Minami, K. Norisuye, S. Umetani, Multielemental determination of GEOTRACES key trace metals in seawater by ICPMS after preconcentration using an ethylenediaminetriacetic acid chelating resin. *Anal. Chem.* **80**, 6267–6273 (2008).
52. M. Frank, D. Porcelli, P. Andersson, M. Baskaran, G. Björk, P. W. Kubik, B. Hattendorf, D. Guenther, The dissolved Beryllium isotope composition of the Arctic Ocean. *Geochim. Cosmochim. Acta* **73**, 6114–6133 (2009).
53. T. J. Suhrhoff, J. Rickli, M. Christl, E. G. Vologina, V. Pham, M. Belhadj, E. V. Sklyarov, C. Jeandel, D. Vance, Source to sink analysis of weathering fluxes in Lake Baikal and its watershed based on riverine fluxes, elemental lake budgets, REE patterns, and radiogenic (Nd, Sr) and $^{10}Be/^{9}Be$ isotopes. *Geochim. Cosmochim. Acta* **321**, 133–154 (2022).
54. J. McManus, W. M. Berelson, G. P. Klinkhammer, D. E. Hammond, C. Holm, Authigenic uranium: Relationship to oxygen penetration depth and organic carbon rain. *Geochim. Cosmochim. Acta* **69**, 95–108 (2005).
55. M. Kusakabe, T. L. Ku, J. R. Southon, J. S. Vogel, D. E. Nelson, C. I. Measures, Y. Nozaki, Distribution of ^{10}Be and ^{9}Be in the Pacific Ocean. *Earth Planet. Sci. Lett.* **82**, 231–240 (1987).
56. P. J. Statham, P. A. Yeats, W. M. Landing, Manganese in the eastern Atlantic Ocean: Processes influencing deep and surface water distributions. *Mar. Chem.* **61**, 55–68 (1998).
57. J. D. Milliman, K. L. Farnsworth, in *River Discharge to the Coastal Ocean – a Global Synthesis* (Cambridge Univ. Press, 2011).
58. B. Campforts, V. Vanacker, J. Vanderborght, S. Baken, E. Smolders, G. Govers, Simulating the mobility of meteoric ^{10}Be in the landscape through a coupled soil-hillslope model (Be2D). *Earth Planet. Sci. Lett.* **439**, 143–157 (2016).
59. J. Gaillardet, J. Viers, B. Dupré, Trace Elements in River Waters, in *Treatise on Geochemistry*, H. D. Holland, K. K. Turekian, Eds. (Elsevier, Oxford, ed. 2, 2014), pp. 195–235.
60. C. Shen, J. Beer, P. Kubik, W. Sun, T. Liu, K. Liu, ^{10}Be in desert sands, falling dust and loess in China. *Nucl. Instrum. Methods Phys. Res., Sect. B* **268**, 1050–1053 (2010).
61. F. von Blanckenburg, J. Bouchez, H. Wittmann, Earth surface erosion and weathering from the ^{10}Be (meteoric)/^{9}Be ratio. *Earth Planet. Sci. Lett.* **351**–**352**, 295–305 (2012).
62. C.-T. A. Chen, Chemical and physical fronts in the Bohai, Yellow and East China seas. *J. Mar. Sys.* **78**, 394–410 (2009).
63. J. J. Middelburg, K. Soetaert, P. M. J. Herman, Empirical relationships for use in global diagenetic models. *Deep Sea Res. Part I* **44**, 327–344 (1997).
64. K. M. Costa, C. T. Hayes, R. F. Anderson, F. J. Pavia, A. Bausch, F. Deng, J.-C. Dutay, W. Geibert, C. Heinze, G. Henderson, C. Hillaire-Marcel, S. Hoffmann, S. L. Jaccard, A. W. Jacobel, S. S. Kienast, L. Kipp, P. Lerner, J. Lippold, D. Lund, F. Marcantonio, D. McGee, J. F. McManus, F. Mekik, J. L. Middleton, L. Missiaen, C. Not, S. Pichat, L. F. Robinson, G. H. Rowland, M. Roy-Barman, A. Tagliabue, A. Torfstein, G. Winckler, Y. Zhou, ^{230}Th normalization: New insights on an essential tool for quantifying sedimentary fluxes in the modern and quaternary ocean. *Paleoceanogr. Paleoclimatol.* **35**, e2019PA003820 (2020).
65. B. Deng, J. Zhang, Y. Wu, Recent sediment accumulation and carbon burial in the East China Sea. *Global Biogeochem. Cycles* **20**, GB3014 (2006).
66. S. Emerson, V. Grundmanis, D. Graham, Carbonate chemistry in marine pore waters: MANOP sites C and S. *Earth Planet. Sci. Lett.* **61**, 220–232 (1982).
67. D. J. Burdige, Preservation of organic matter in marine sediments: Controls, mechanisms, and an imbalance in sediment organic carbon budgets? *Chem. Rev.* **107**, 467–485 (2007).
68. G. Song, S. Liu, Z. Zhu, W. Zhai, C. Zhu, J. Zhang, Sediment oxygen consumption and benthic organic carbon mineralization on the continental shelves of the East China Sea and the Yellow Sea. *Deep Sea Res. Part II* **124**, 53–63 (2016).
69. W. M. Berelson, D. E. Hammond, D. O'Neill, X. m. Xu, C. Chin, J. Zukin, Benthic fluxes and pore water studies from sediments of the central equatorial north Pacific: Nutrient diagenesis. *Geochim. Cosmochim. Acta* **54**, 3001–3012 (1990).
70. D. Kadko, A multitracer approach to the study of erosion in the northeast equatorial Pacific. *Earth Planet. Sci. Lett.* **63**, 13–33 (1983).
71. N. M. Mahowald, A. R. Baker, G. Bergametti, N. Brooks, R. A. Duce, T. D. Jickells, N. Kubilay, J. M. Prospero, I. Tegen, Atmospheric global dust cycle and iron inputs to the ocean. *Global Biogeochem. Cycles* **19**, GB4025 (2005).
72. C. I. Measures, J. M. Edmond, The geochemical cycle of ^{9}Be: A reconnaissance. *Earth Planet. Sci. Lett.* **66**, 101–110 (1983).
73. E. T. Brown, J. M. Edmond, G. M. Raisbeck, D. L. Bourlès, F. Yiou, C. I. Measures, Beryllium isotope geochemistry in tropical river basins. *Geochim. Cosmochim. Acta* **56**, 1607–1624 (1992).
74. W. Kong, L. Zhou, G. Aumaître, D. Bourlès, K. Keddadouche, Dissolved and particulate beryllium isotopes in the Pearl River estuary: Their geochemical behavior in estuarine water and potential contributions from anthropogenic sources. *Front. Mar. Sci.* **8**, 689890 (2021).
75. M. Kusakabe, T. L. Ku, J. R. Southon, L. Shao, J. S. Vogel, D. E. Nelson, S. Nakaya, G. L. Cusimano, Be isotopes in rivers/estuaries and their oceanic budgets. *Earth Planet. Sci. Lett.* **102**, 265–276 (1991).
76. C. Neal, Dissolved and acid available particulate beryllium in eastern UK surface waters. *Sci. Total Environ.* **314**–**316**, 185–208 (2003).
77. C. Neal, Dissolved beryllium in rainfall, stream and shallow groundwaters in the Upper River Severn catchments, Plynlimon, mid Wales. *Sci. Total Environ.* **314**–**316**, 171–184 (2003).
78. M. E. Åström, C. Yu, P. Peltola, J. K. Reynolds, P. Österholm, M. I. Nystrand, A. Augustsson, J. J. Virtasalo, L. Nordmyr, A. E. K. Ojala, Sources, transport and sinks of beryllium in a coastal landscape affected by acidic soils. *Geochim. Cosmochim. Acta* **232**, 288–302 (2018).

Acknowledgments: K.D. thanks A. Corey for the help with lab work. Participants of RV Alkor Cruise AL543 are thanked for their contribution to the sampling. **Funding:** This work was supported by ETH Zürich Postdoctoral Fellowship 20-1 FEL-24 (K.D.); National Key R&D Program of China (no. 2022YFF0800504); National Natural Science Foundation of China (nos. 42230410 and 42006059); German Research Foundation (DFG), Emmy-Noether-Nachwuchsforschergruppe ICONOX (F.S.); and U.S. National Science Foundation (no. OC-1657690 to S.S. and no. OC-1657832 to J.M.). **Author contributions:** Conceptualization: K.D. and D.V. Methodology: K.D., J.R., T.J.S., and J.D. Investigation: K.D. Resources: S.S., J.M., F.S., and S.Y. Visualization: K.D. Supervision: D.V. Funding acquisition: D.V. and K.D. Writing (original draft): K.D. Writing (review and editing): D.V., J.R., T.J.S., J.D., F.S., S.Y., and J.M. **Competing interests:** The authors declare that they have no competing interests. **Data and materials availability:** All data needed to evaluate the conclusions in the paper are present in the paper and/or the Supplementary Materials.

Submitted 22 December 2022
Accepted 5 May 2023
Published 7 June 2023
10.1126/sciadv.adg3702